Inorganic Chemistry

Article

pubs.acs.org/IC

Metallic Yb_2AuGe_3: An Ordered Superstructure in the AlB_2-Type Family with Mixed-Valent Yb and a High-Temperature Phase Transition

Sebastian C. Peter and Sumanta Sarkar

New Chemistry Unit, Jawaharlal Nehru Centre for Advanced Scientific Research, Jakkur, Bangalore, 560064, India

Mercouri G. Kanatzidis*

Department of Chemistry, Northwestern University, 2145 North Sheridan Road, Evanston, Illinois 60208, United States and Materials Science Division, Argonne National Laboratory, Argonne, Illinois 60439, United States

Supporting Information

ABSTRACT: The intermetallic compound Yb_2AuGe_3 was synthesized from indium flux. Yb_2AuGe_3 crystallizes in the orthorhombic Ca_2AgSi_3-type structure which is an ordered superstructure of the AlB_2 structure type. The structure was refined in the *Fmmm* space group with lattice parameters a = 8.5124(17) Å, b = 14.730(3) Å, c = 8.4995(17) Å. Temperature-dependent powder X-ray diffraction studies show that Yb_2AuGe_3 undergoes a phase transition from orthorhombic to hexagonal upon heating above 773 K. The compound shows weak paramagnetism that derives from a combination of Curie and Pauli paramagnetism with a magnetic moment value of 0.33(2) μ_B/Yb atom. Magnetic ordering was not observed down to 2 K. Yb_2AuGe_3 is metallic, and at low temperature the resistivity varies as T^2, indicating possible Fermi liquid behavior. Heat capacity measurements suggest that Yb_2AuGe_3 is possibly a moderate heavy fermion system.

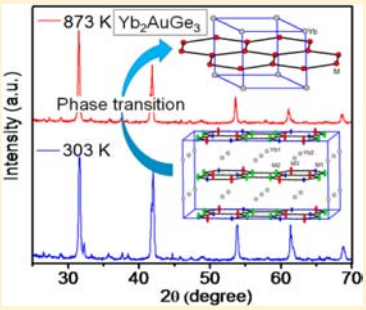

1. INTRODUCTION

Rare-earth-based ternary intermetallics having general formula RE_2TX_3 (where RE = rare earths; T = transition metal, X = terellide or tetrellide) crystallize in ordered superstructures of the AlB_2 structure type.[1] These compounds are interesting for their structural and crystallographic[2] aspects and also in terms of their ability to exhibit novel and unusual physical properties. For example, Tb_2PdSi_3 and Er_2PdSi_3 are spin glasses,[3] Tb_2PdSi_3 shows quasi-one-dimensional magnetic behavior,[4] Tb_2CuGe_3 presents multiple magnetic transitions,[5] Y_2PdGe_3 and its substituted variant with platinum in the palladium position become superconductors,[6,7] Gd_2PdSi_3 exhibits magnetocaloric effect (MCE) below 50 K[8] and large negative magnetoresistance,[9] Eu_2CuSi_3 shows large magnetoresistance above its Curie temperature,[10] Ce_2CoSi_3, Ce_2RhSi_3, and $Ce_2Rh_{1-x}Co_xSi_3$ compounds show the Kondo effect, etc.[11−13]

RE_2TX_3 Intermetallics can be derived from the prototype AlB_2 structure by Bärnighausen formalism applying three different types of symmetry operations like *klassengleiche* (k), *translationengleiche* (t), and *isomorphic* transitions (i).[14,15] Although there are a few reports with other transition metals such as Ce_2TSi_3,[16] with T = (Cr, Mn, Fe, Co, or Ni)$_x$(Pd or Au)$_{1-x}$, Ce_2IrSi_3,[17] rare-earth-based silicides with second- or third-row transition metals, especially, rhodium,[11,12,18] palladium,[3,5,19] and platinum[20] are the most widely studied intermetallics in this series.

Many of these phases, such as RE_2PdSi_3 (RE = Gd, Tb, Dy, Ho) crystallize in hexagonal structures or in its more or less ordered derivatives as, for example, Eu_2AuGe_3,[21] which crystallizes in orthorhombic superstructure in *Fmmm* space group. In RE_2TX_3, the RE atoms occupy the aluminum position while the T and X atoms form the two-dimensional infinite hexagonal network. Depending on the substituting atoms, the two-dimensional net may be puckered to different extents.[1] Because of this kind of shared occupancy at crystallographic positions of T and Si atoms and topological frustration in a triangular sublattice of magnetic atoms, these phases exhibit a wide variety of magnetic behavior.[22−31]

The ability to obtain large single-crystal specimens from the metal flux technique[32−34] has much contributed to our understanding of the detailed structures of these compounds. Assignment of the space group to Er_2RhSi_3 is a classic example on this context. X-ray diffraction data on powder samples suggested a noncentrosymmetric space group ($P62c$) for Er_2RhSi_3,[18] but later single-crystal X-ray diffraction (XRD) studies confirmed the centrosymmetric space group $P\bar{6}_3/mmc$, which also corresponds to the hexagonal crystal system.[35]

We targeted the synthesis of single-crystal Yb_2AuGe_3 using indium as the metal flux because relatively few germanides exist in the RE_2TX_3 series compared to silicides[16−20] and in the

Received: June 5, 2012
Published: September 24, 2012

   dx.doi.org/10.1021/ic301197w | *Inorg. Chem.* 2012, 51, 10793−10799

context of our previous work on Yb intermetallics.[36−49] This is the first ytterbium-based compound within the RE_2TX_3 family that crystallizes in the ordered superstructure of AlB_2 structure type. Among the rare earths, the Yb-containing compounds have particular scientific interest because they can exhibit two energetically similar electronic configurations: the magnetic Yb^{3+} ($4f^{13}$) and the nonmagnetic Yb^{2+} ($4f^{14}$) one.[50] In this case, the roles of the 4f electron and 4f hole can be interchanged, and many phenomena, such as intermediate valence, Kondo effect, or heavy fermion behavior and even structural transformation can be observed.[49,51−55] $YbRh_2Si_2$ is a classical example of mixed-valent Yb-based compounds that shows heavy fermion behavior.[55,56] Yb_2AuGe_3 shows a phase transition at higher temperature as observed in temperature-dependent powder XRD studies. It is worthwhile to mention in this context that reports in this series containing gold as a transition metal are also rare apart from our recent report on Eu_2AuGe_3.[21] Our magnetic measurements suggest that Yb_2AuGe_3 has Yb atoms in a mixed-valent state and the material is metallic, while temperature-dependent electrical resistivity measurements at low temperature indicate possible Fermi liquid behavior. Finally, heat capacity data suggest moderate heavy fermion behavior for Yb_2AuGe_3.

2. EXPERIMENTAL SECTION

2.1. Reagents. The following reagents were used as purchased without further purification: Yb (in the form of metal pieces cut from metal chunk, 99.9% Alfa Aesar), Au (pieces, 99.99% Alfa Aesar), Ge (ground from metal pieces 99.999% Alfa Aesar), and In (tear drops 99.99% Alfa Aesar).

2.2. Synthesis. *Method 1.* Single crystals of Yb_2AuGe_3 were obtained by combining 3 mmol of the ytterbium metal, 2 mmol of gold, 6 mmol of germanium, and 45 mmol of indium in an alumina (Al_2O_3) crucible under an inert (argon) atmosphere inside a glovebox. The crucible was placed in a 13 mm quartz tube and flame sealed under vacuum of 10^{-3} Torr to prevent oxidation during heating. The tube was then placed in a vertically aligned tube furnace and heated to 1273 K over a period of 10 h, maintained at that temperature for 5 h to allow proper homogenization, followed by cooling to 1123 K in 2 h, and held at that temperature for 48 h. Finally, the system was allowed to cool slowly to room temperature in 48 h. The reaction product was isolated from the excess In flux by heating at 623 K and subsequent centrifugation through a coarse frit. Any remaining flux was removed by immersion and sonication in glacial acetic acid for 24 h. The final crystalline product was rinsed with water and dried with acetone in a vacuum oven at 350 K overnight. This method produced the target compound with ∼98% purity and in a yield of ∼95% on the basis of the initial amount of Yb metal used in the reaction. Side products were very small amounts (<2% of the overall product obtained) of Ge and residual In metal flux, which was quite unavoidable. Yb_2AuGe_3 is stable in air and moisture with no decomposition observed even after several months. Several crystals, which grew as metallic silver rods with an average size of 5−6 mm, were carefully selected for elemental analysis, structure characterization, and physical measurements reported in this article. This method was well reproducible under the same experimental conditions.

Method 2. Ytterbium, gold, and germanium were mixed in the ideal 2:1:3 atomic ratios and sealed in tantalum ampules under an argon atmosphere in an arc melting apparatus. The tantalum ampules were subsequently placed in a water-cooled sample chamber of an induction furnace (EasyHeat induction heating system, model 7590), first rapidly heated to ca. 1250 K, and kept at that temperature for 10 min. Finally, the temperature was lowered to 1000 K, and the sample was annealed at that temperature for another 30 min, followed by quenching by switching off the power supply. The brittle product could easily be separated from the tantalum tube. No reaction with the container was observed. The obtained compound was pure up to the level of powder XRD.

2.3. X-ray diffraction. To determine the phase identity and purity, the powder X-ray diffraction pattern of Yb_2AuGe_3 was collected at room temperature on a Bruker D8 Discover X-ray diffractometer with a Cu Kα X-ray source (λ = 1.5406 Å), equipped with a position-sensitive detector, and compared to the pattern calculated from single-crystal structure refinement. Comparison of the powder pattern with the simulated pattern obtained from single-crystal data is shown in the Supporting Information (Figure S1). The powder X-ray diffraction data of Yb_2AuGe_3 could be indexed on the basis of an orthorhombic unit cell with lattice parameters a = 8.52 Å, b = 14.74 Å, and c = 8.49 Å.

Temperature-dependent powder XRD data were collected in the same instrument under vacuum condition (10^{-6} Torr pressure) on a tantalum plate in the temperature range 303−1073 K (both heating and cooling). Comparison of powder XRD patterns at temperatures of 303, 773 and 873 K is shown in Figure 4 (all plots collected are not shown for simplicity). The phase transition occurs over a broad range of temperature above 773 K. The powder XRD pattern obtained at 873 K was compared with the simulated pattern of the hexagonal substructure (shown in Figure S2, Supporting Information). Figure S3, Supporting Information, shows the progressively increasing intensity of the substructure peaks which are marked by black arrows. One of the superstructure peaks corresponding to the (0 4 2) plane is shown in the inset of Figure S3, Supporting Information; the peak intensity decreased with increasing temperature, and it completely vanished at 873 K.

X-ray diffraction data on a Yb_2AuGe_3 single crystal were collected at room temperature using a STOE IPDS 2T (with additional capability of 2θ swing of the detector) diffractometer with graphite-monochromatized Mo Kα (λ = 0.71073 Å) radiation. The X-AREA (X-RED and X-SHAPE within) package suite[57] was used for data extraction and integration and to apply numerical absorption corrections. Details on the crystallographic data are given in Table 1.

The room temperature data set of Yb_2AuGe_3 was compatible with space group *Fmmm*. The atomic parameters of Ca_2AgSi_3 were then taken as starting values, and the structure was refined with SHELXL-97 (full-matrix least-squares on F^2)[58] with anisotropic atomic displacement parameters for all atoms. Results of the structure refinement are summarized in Table 1. Atomic coordinates and interatomic distances are listed in Tables 2 and 3.

2.4. Structure Refinement. Single-crystal data of Yb_2AuGe_3 showed an orthorhombic cell, and systematic extinctions were compatible with the space group *Fmmm*. The Ca_2AgSi_3 structure type,[59] a superstructure of AlB_2 type, was already evident from the powder X-ray diffraction data. The atomic parameters of Ca_2AgSi_3 were taken as starting parameters, and the structure was refined using SHELXL-97 (full-matrix least-squares on F^2)[60] with anisotropic atomic displacement parameters for all atoms. As a check for the correct composition, the occupancy parameters were refined in a separate series of least-squares cycles. Initially, there were five crystallographically different positions in the Yb_2AuGe_3 structure: two for each Yb and Ge atom and one for the Au atom. During isotropic refinement it was observed that the atomic displacement parameters of the gold and germanium atoms were anomalously large. Furthermore, the refinement was largely unsatisfactory, giving relatively high residuals (R_1 > 12%) and large electron density residuals (19−20 e Å^{-3}) around the gold and germanium atoms. Anisotropic refinement did not improve the refinement and also resulted in abnormal cigar-shaped gold and germanium atomic displacement ellipsoids (U_{22} = 0.50 Å^2). The anomalous atomic displacement parameter could not be resolved by subsequent refinement of the occupancy parameters. All features indicated a crystallographic disorder associated with the Ge and Au atoms. Consequently, gold and germanium atoms were refined by mixing germanium and gold, respectively, which makes the compound slightly of different stochiometry. Au/Ge mixing was previously reported on NaAuGe[61] and EuAuGe[62,63] and a large family of compounds, RAuGe (R = Sc, Y, La−Nd, Sm, and Gd−Lu).[64−67] The resulting atomic displacement parameters of mixed positions became

dx.doi.org/10.1021/ic301197w | Inorg. Chem. 2012, 51, 10793−10799

Table 1. Crystal Data and Structure Refinement for Yb_2AuGe_3 at 293(2) K[a]

empirical formula	Yb_2AuGe_3
fw	764.39
temp.	293(2) K
wavelength	0.71073 Å
cryst syst	orthorhombic
space group	*Fmmm*
unit cell dimens	a = 8.5124(17) Å, α = 90.00°
	b = 14.730(3) Å, β = 90.00°
	c = 8.4995(17) Å, γ = 90.00°
vol.	1065.7(4) Å^3
Z	8
density (calcd)	9.528 g/cm^3
abs coeff	79.326 mm^{-1}
F(000)	2531
cryst size	0.12 × 0.10 × 0.08 mm^3
θ range for data collection	4.79−34.26°
index ranges	$-11 \le h \le 13$, $-23 \le k \le 23$, $-12 \le l \le 13$
reflns collected	3715
independent reflns	640 [R_{int} = 0.0982]
completeness to θ = 34.26°	98.5%
refinement method	full-matrix least-squares on F^2
data/restraints/params	640/0/26
goodness-of-fit	1.188
final R indices [>2σ(I)]	R_{obs} = 0.0544, wR_{obs} = 0.1201
R indices [all data]	R_{all} = 0.0567, wR_{all} = 0.1212
extinction coefficient	0.00019(4)
largest diff. peak and hole	8.003 and −11.322 e·Å^{-3}

[a] $R = \Sigma||F_o| - |F_c||/\Sigma|F_o|$, $wR = \{\Sigma[w(|F_o|^2 - |F_c|^2)^2]/\Sigma[w(|F_o|^4)]\}^{1/2}$, and calc $w = 1/[\sigma^2(F_o^2) + (0.0306P)^2 + 142.9431P]$ where $P = (F_o^2 + 2F_c^2)/3$.

Table 2. Atomic Coordinates and Equivalent Isotropic Displacement Parameters (Å^2 × 10^3) for Yb_2AuGe_3 at 293(2) K with Estimated Standard Deviations in Parentheses

label	x	y	z	occupancy	U_{eq}[a]
Yb(1)	0	0	0.2506(1)	1	14(1)
Yb(2)	0.2500	0.2500	0.2500	1	14(1)
Au(1)	0	6667(1)	0	0.709(8)	14(1)
Ge(1)	0	6667(1)	0	0.291(8)	14(1)
Au(2)	0.2486(2)	0.0829(1)	0	0.137(6)	27(1)
Ge(2)	0.2486(2)	0.0829(1)	0	0.863(6)	27(1)
Au(3)	0	0.1656(2)	0	0.045(11)	37(1)
Ge(3)	0	0.1656(2)	0	0.955(11)	37(1)

[a] U_{eq} is defined as one-third of the trace of the orthogonalized U_{ij} tensor.

well behaved, and the final difference maps showed residuals that were reasonably acceptable. Relatively large displacement parameters of M2 and M3 positions (i.e., along the c axis) indicate a further symmetry reduction at low temperature similar to our previous report on Eu_2AuGe_3.[21] However, it was not observed in the single-crystal data obtained at the lowest temperature and no hint from the physical properties (discussed below) as we observed in Eu_2AuGe_3 compounds. Nevertheless, when we attempted to remove the mirror plane along the c axis and refine the crystal structure in *Fmm*2 space group, we obtained large residuals and atomic displacement parameters. Our attempts to refine the structure in the *F*222 space group also were not successful. With all these we conclude that Yb_2AuGe_3 gives the best possible refinement within the *Fmmm* space group and Ca_2AgSi_3-type structure. Final refinement gives an atomic ratio of $Yb_2Au_{1.029}Ge_{2.971}$. Data collection and refinement parameters are summarized in Table 1.

Table 3. Anisotropic Displacement Parameters (Å^2 × 10^3) for Yb_2AuGe_3 at 293(2) K with Estimated Standard Deviations in Parentheses[a]

label	U_{11}	U_{22}	U_{33}	U_{12}	U_{13}	U_{23}
Yb(1)	15(1)	12(1)	15(1)	0	0	0
Yb(2)	15(1)	13(1)	16(1)	0	0	0
Au(1)	9(1)	5(1)	29(1)	0	0	0
Ge(1)	9(1)	5(1)	29(1)	0	0	0
Au(2)	12(1)	9(1)	60(2)	0(1)	0	0
Ge(2)	12(1)	9(1)	60(2)	0(1)	0	0
Au(3)	13(1)	8(1)	89(2)	0	0	0
Ge(3)	13(1)	8(1)	89(2)	0	0	0

[a] The anisotropic displacement factor exponent takes the form $-2\pi^2[h^2a^{*2}U_{11} + ... + 2hka^*b^*U_{12}]$.

Atomic coordinates and equivalent atomic displacement parameters, anisotropic atomic displacement parameters, and important bond lengths are listed in Tables 2, 3, and 4, respectively.

Table 4. Selected Bond Lengths [Angstroms] for Yb_2AuGe_3 at 293(2) K with Estimated Standard Deviations in Parentheses[a]

label	distances	label	distances
M(2)−M(3)	2.4411(16)	M(1)−Yb(1)	3.2443(9)
M(2)−M(2)	2.443(2)	M(1)−Yb(2)	3.2478(5)
M(1)−M(3)	2.470(2)	M(2)−Yb(1)	3.2506(11)
M(1)−M(2)	2.4709(13)	M(2)−Yb(2)	3.2515(10)
M(3)−Yb(1)	3.2382(17)	M(3)−Yb(2)	3.2543(9)
M(2)−Yb(1)	3.2413(11)		

[a] M1 = Au1 + Ge1, M2 = Au2 + Ge2, and M3 = Au3 + Ge3.

2.5. Elemental Analysis. A quantitative microanalysis on Yb_2AuGe_3 was performed with a FEI NOVA NANOSEM 600 instrument equipped with an EDAX instrument. Data were acquired with an accelerating voltage of 20 kV and a 60 s accumulation time. A typical metallic rod-shaped single crystal of Yb_2AuGe_3 obtained from the flux reaction is shown in Figure 1. EDS analysis was performed using *P*/*B*-*ZAF* standardless analysis (where Z = atomic no. correction factor, A = absorption correction factor, F = fluorescence factor, P/B = peak to background model) on visibly clean surfaces of the Yb_2AuGe_3 crystal. Analysis gave the atomic composition of 31% Yb, 20% Au, and 48% Ge, which is close to the composition obtained from single-crystal X-ray diffraction results ($Yb_2Au_{1.029}Ge_{2.971}$).

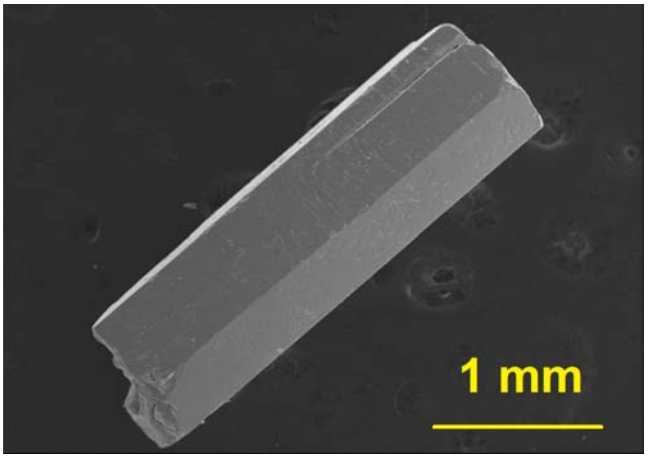

Figure 1. SEM image of a single crystal of Yb_2AuGe_3 grown from In metal flux.

dx.doi.org/10.1021/ic301197w | *Inorg. Chem.* 2012, 51, 10793−10799

2.6. Magnetic Measurements. Magnetic susceptibility measurements were carried out with a Quantum Design MPMS SQUID magnetometer. Single crystals of Yb_2AuGe_3 were loaded randomly without grounding into gelatin capsules, mounted in a plastic straw, and affixed to the end of a carbon fiber rod. Temperature dependent data were collected between 2 and 300 K, with an applied magnetic field of 1000 Oe. In a typical measurement, data were collected while cooling the sample from 300 to 2 K. Field-dependent magnetic measurements were acquired at 5 K with field sweeping from −50 to +50 kG for Yb_2AuGe_3. Raw data were corrected for the sample holder (straw) contribution.

2.7. Electrical Resistivity. Resistivity measurements performed on selected single crystals of Yb_2AuGe_3 were measured over the temperature range of 2−300 K using a four-probe dc technique with contacts made with silver paste. Measurements were conducted using a Quantum Design PPMS magnetometer. Results were reproducible for several crystals.

2.8. Specific Heat. Heat capacity (C_p) measurements were performed on selected single crystals of Yb_2AuGe_3 by relaxation method using a commercial Quantum Design Physical Property Measurement System (QD-PPMS). Sample was glued to a calibrated HC-puck using Apiezon N grease. C_p was measured in the 1.8−50 K range without applied fields (H).

3. RESULTS AND DISCUSSIONS

3.1. Crystal Structure. Yb_2AuGe_3 crystallizes in the Ca_2AgSi_3-type structure which is an ordered superstructure of the AlB_2 family. This is the first example of Yb-based germanide in the RE_2TX_3 family that crystallizes in an ordered superstructure of AlB_2. In Yb_2AuGe_3, M1, M2, and M3 atoms form hexagons that form graphite-like layers (Figure 2). The shortest

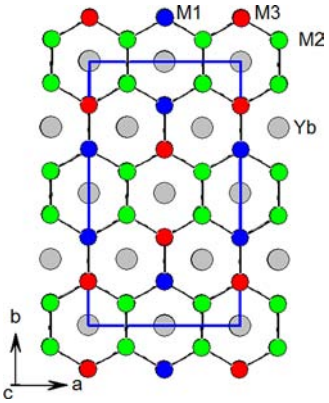

Figure 2. View of the Yb_2AuGe_3 structure approximately along the b axis; M1 = Au1 + Ge1, M2 = Au2 + Ge2, and M3 = Au3 + Ge3. Ytterbium atoms are embedded in the two-dimensional hexagonal $[AuGe_3]$ networks.

distance between the hexagonal layers is 4.2498(8) Å for Yb_2AuGe_3. Yb atoms are intercalated between the $[M_6]$ layers. The layers are stacked along the b axis in an eclipsed fashion as shown in Figure 3. Also, the shortest distance between the Yb and the M (3.2382 Å) is slightly larger than the Yb−Ge and Yb−Au distances in other intermetallics; this suggests[68] a weak interaction between them. The Ge−Ge bond distances (2.4313−2.4738 Å) are within the normal range of the Ge−Ge covalent bond length, 2.45 Å.[69] The short M1−M2 distance is a hint of puckering of the M_6 layer, but slightly large atomic displacement parameters of M3 along the b axis suggest a certain amount of disorder in the stacking registry of the $[M_6]$ layers. We hypothesized that this disorder could induce a temperature-dependent phase transition in Yb_2AuGe_3 similar to

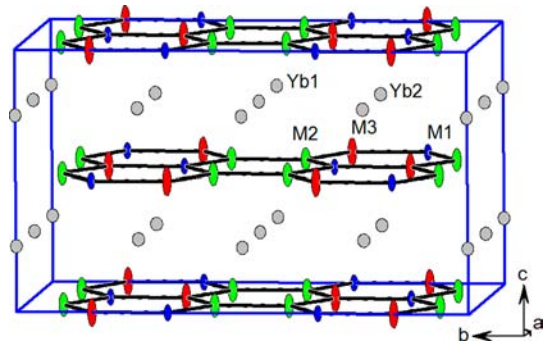

Figure 3. View of the Yb_2AuGe_3 structure approximately along the a axis; M1 = Au1 + Ge1, M2 = Au2 + Ge2, and M3 = Au3 + Ge3.

the one observed in Eu_2AuGe_3[21] at ∼130 K from orthorhombic to a monoclinic system. However, low-temperature single-crystal data analysis for Yb_2AuGe_3 down to 4 K did not show any hint of phase transformation, and we did not observe anomalies in electrical resistivity data in the temperature range 2−300 K (shown in Physical Properties section below).

A phase transition was found at high temperature as observed in the powder XRD data from 303 to 1073 K (Figure 4). Above

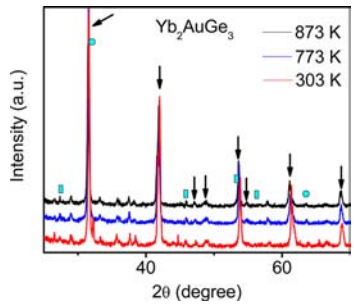

Figure 4. Comparison of powder XRD patterns of Yb_2AuGe_3 at 303, 773, and 873 K. Peaks which originate from the substructure (hexagonal structure) of the compound are shown by arrows. Unreacted Ge (cubic, $Fd\bar{3}m$ space group) and In (tetragonal, $I4/mmm$ space group) peaks are shown by rectangular and circular markups, respectively. Remaining peaks correspond to superstructure diffractions.

873 K, Bragg peaks corresponding to the superstructure reflections progressively decreased in intensity and peaks which correspond to the substructure (hexagonal) increased. In order to simulate the powder pattern we removed the superstructure reflections from the single-crystal XRD data and refined the substructure of Yb_2AuGe_3 in the AlB_2, $P6/mmm$ space group, and lattice constants are $a = b = 4.2476$ (6) Å, $c = 4.2376(8)$ Å. The simulated powder pattern obtained is in agreement with the experimental powder diffraction pattern obtained at or above 873 K.

3.2. Physical Properties. *Magnetic Measurements.* Figure 5 shows the temperature dependence of the molar magnetic susceptibility (χ_m) of a ground sample of Yb_2AuGe_3 measured from 3 to 300 K with an applied magnetic field of 1000 Oe. No long-range magnetic order could be observed down to 3 K; however there is an upturn in the magnetic susceptibility data around 50 K, suggesting paramagnetic behavior.[70] From the linear region of the inverse susceptibility plot (50−300 K) the calculated value for the paramagnetic Curie−Weiss temperature (θ_p) is 10.9 (1) K, suggesting weak

dx.doi.org/10.1021/ic301197w | Inorg. Chem. 2012, 51, 10793−10799

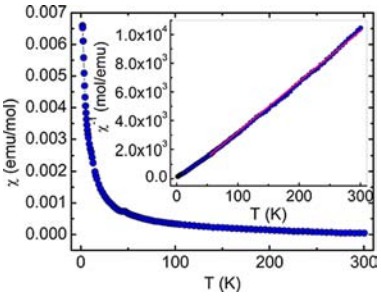

Figure 5. Magnetic susceptibility (χ = M/H) as a function of temperature for Yb_2AuGe_3 (polycrystalline) sample measured in a dc field of 1 kOe. (Inset) Inverse magnetic susceptibility (χ^{-1} = H/M).

ferromagnetic coupling between the Yb moments. The estimated effective moment of 0.33(2) μ_B is only ~7% of the value expected for the free-ion Yb^{3+}, 4.54 μ_B. This indicates that the compound contains both Yb^{2+} and Yb^{3+} moieties. The field dependence of the magnetization $M(H)$ for Yb_2AuGe_3 ground sample at 5 K can be found in Figure 6 exhibiting linear

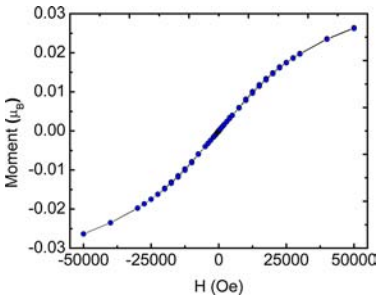

Figure 6. Magnetization as a function of applied magnetic field at 5 K for a polycrystalline sample of Yb_2AuGe_3.

behavior up to about 24 kG at which point the slope changes continuously until about 50 kG, but no signs of saturation up to highest attainable field of 50 kG were observed.

Resistivity. The electrical resistivity $\rho(T)$ of Yb_2AuGe_3 in the range 2−300 K is presented in Figure 7. The resistivity data measured on single crystals along the *c* axis and at zero applied field reveal metallic conductivity with a room-temperature resistivity value ρ(300 K) of 1600 $\mu\Omega$ cm. This value of room-temperature resistivity, ρ(300) for Yb_2AuGe_3, was comparable with that previously reported for Eu_2AuGe_3 (947 $\mu\Omega$ cm). To further investigate the correlative nature of the conduction

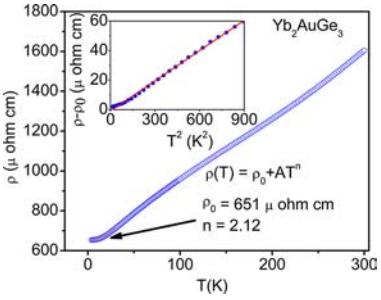

Figure 7. Temperature-dependent electrical resistivity $\rho(T)$ of a single-crystal sample of Yb_2AuGe_3 in the temperature range 2−300 K. Low-temperature data has been fitted to the power law, $\rho = \rho 0 + AT^n$. Values obtained from the fit are shown in the figure. Plot of $\rho-\rho_0$ vs T^2 showing a linear relationship is shown as an inset.

electrons in the compound, we fitted the $\rho(T)$ vs T curve with the power-law function $\rho(T) = \rho_0 + AT^n$, where $\rho(T)$ is the resistivity at any temperature T, ρ_0 is the residual resistivity, and A and n are fitting parameters in the low-temperature range (2−30 K).[71] According to Fermi liquid theory, at low temperatures the resistivity varies as $\rho = \rho_0 + AT^2$.[72] Experimentally it has been observed that when electron−electron scattering dominates over electron−phonon scattering, $\rho \propto T^2$.[73] The nonlinear fitting of the curve in this temperature range gave a ρ_0 value of 651 μohm cm and n = 2.12.[47,74] Thus, in the prescribed temperature range the power law is reduced to $\rho(T) = \rho_0 + AT^2$, which are consistent with the Fermi liquid behavior. To better illustrate the Fermi liquid behavior in Yb_2AuGe_3, the resistivity data are plotted as $[\rho(T) - \rho_0]$ vs T^2 as an inset in Figure 7. The linearity of the data proves that the compound Yb_2AuGe_3 has a strongly correlated Fermi liquid ground state at low temperature. In this context, it is worthwhile to mention that the compound CeRuSi, a "moderate heavy fermion" with a γ value[75] of 180 mJ/mol·K^2, also shows Fermi liquid behavior.[76] The resistivity varies linearly with T^2.

Heat Capacity. The specific heat from 1.8 to 50 K for Yb_2AuGe_3 is shown in Figure 8. The absence of long-range

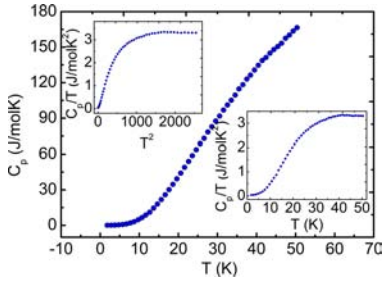

Figure 8. Heat capacity (C_p) of Yb_2AuGe_3 measured from 1.8 to 50 K. (Inset) C_p/T vs T and C_p/T vs T^2.

magnetic ordering in Yb_2AuGe_3 was already observed from the magnetic susceptibility measurements. Further evidence can be found in the plot of specific heat vs temperature. C_p decreases as the temperature is lowered. $C_p(T)$ does not exhibit any anomaly, thus ruling out any type of long-range phase transitions. $C_p(T)$ has been shown in different forms as insets in Figure 8. The observed specific heat at low temperatures can be described by the equation $C_p = \gamma T + \beta T^3$, which shows that the total specific heat of the sample is comprised of the contributions from the electronic part (coefficient of electronic specific heat, γ) as well as the lattice part (β). Thus, at low temperatures C_p should vary as a function of T^3; the plot of C_p/T vs T^2 should be a straight line.[77] Such a plot is convenient for calculating the values of both γ and β.

A fit from the plot of C_p/T vs T^2 (T = 7−15 K) resulted in a value of γ = 109 mJ/mol K^2, suggesting a moderate heavy fermion material according to the arbitrary classification of these compounds into "light", "moderate", and classical heavy fermions with γ values lying in the range of ~50−60, 100−400, and >400 mJ/mol K^2, respectively.[78] This value of electronic specific heat compares well with the ones found in other mixed or intermediate valent compounds such as $YbNi_2Ge_2$, $YbRh_2Si_2$, and $Yb_2Co_3Ga_9$.[79,80] The Debye temperature, Θ_D, calculated using the following equation, was 157 K, normal for Yb-based intermetallics. The Debye temperature is a fundamental constant of a solid and a measure of the phonon contribution

dx.doi.org/10.1021/ic301197w | Inorg. Chem. 2012, 51, 10793−10799

toward the overall heat capacity, and a low value of Θ_D indicates a low total heat capacity at low temperatures. Generally materials with heavy atoms exhibit low Debye temperatures.

4. CONCLUDING REMARKS

Single crystals of Yb_2AuGe_3 were obtained from reactions in molten In over a broad range of synthetic conditions. The room-temperature structure (Ca_2AgSi_3 type) was refined from single-crystal diffractometer data. Temperature-dependent powder XRD revealed the phase transformation of Yb_2AuGe_3 above 773 K from orthorhombic to hexagonal symmetry. Magnetization data exhibit the absence of long-range magnetic interactions, and low-temperature resistivity data of Yb_2AuGe_3 are consistent with Fermi liquid behavior. Specific heat measurements show that Yb_2AuGe_3 exhibits what appears to be moderate heavy fermion behavior. These findings call for band-structure calculations, XANES measurements, and neutron diffraction experiments to further probe the electronic structure and its influence on the phase transformation at higher temperature.

■ ASSOCIATED CONTENT

Ⓢ Supporting Information

Crystallographic information files (CIF). This material is available free of charge via the Internet at http://pubs.acs.org.

■ AUTHOR INFORMATION

Corresponding Author

*E-mail: m-kanatzidis@northwestern.edu.

Notes

The authors declare no competing financial interest.

■ ACKNOWLEDGMENTS

We thank JNCASR and DST for financial support. S.S. thanks the CSIR for a research fellowship. S.C.P is thankful for a Ramanujan Fellowship from DST, Government of India. Work at Argonne National Laboratory was supported by the U.S. Department of Energy, Office of Basic Energy Sciences, under Contract DE-AC02-06CH11357.

■ REFERENCES

(1) Hoffmann, R. D.; Pöttgen, R. *Z. Kristallogr.* **2001**, *216*, 127−145.
(2) Tang, F.; Frontzek, M.; Dshemuchadse, J.; Leisegang, T.; Zschornak, M.; Mietrach, R.; Hoffmann, J. U.; Loser, W.; Gemming, S.; Meyer, D. C.; Loewenhaupt, M. *Phys. Rev. B* **2011**, *84*, 104105.
(3) Frontzek, M.; Kreyssig, A.; Doerr, M.; Schneidewind, A.; Hoffmann, J. U.; Loewenhaupt, M. *J. Phys.Condens, Matter* **2007**, *19*, 145276.
(4) Paulose, P. L.; Sampathkumaran, E. V.; Bitterlich, H.; Behr, G.; Loser, W. *Phys. Rev. B* **2003**, *67*, 212401.
(5) Majumdar, S.; Sampathkumaran, E. V. *Solid State Commun.* **2001**, *117*, 645−648.
(6) Sampathkumaran, E. V.; Majumdar, S.; Schneider, W.; Molodtsov, S. L.; Laubschat, C. *Physica B* **2002**, *312*, 152−154.
(7) Iyer, K. K.; Sampathkumaran, E. V. *Physica C* **2007**, *466*, 51−55.
(8) Sampathkumaran, E. V.; Das, I.; Rawat, R.; Majumdar, S. *Appl. Phys. Lett.* **2000**, *77*, 418−420.
(9) Saha, S. R.; Sugawara, H.; Matsuda, T. D.; Sato, H.; Mallik, R.; Sampathkumaran, E. V. *Phys. Rev. B* **1999**, *60*, 12162−12165.
(10) Majumdar, S.; Mallik, R.; Sampathkumaran, E. V.; Rupprecht, K.; Wortmann, G. *Phys. Rev. B* **1999**, *60*, 6770−6774.
(11) Patil, S.; Pandey, S. K.; Medicherla, V. R. R.; Singh, R. S.; Bindu, R.; Sampathkumaran, E. V.; Maiti, K. *J. Phys. Condens. Matter* **2010**, *22*, 255602.
(12) Patil, S.; Medicherla, V. R. R.; Singh, R. S.; Pandey, S. K.; Sampathkumaran, E. V.; Maiti, K. *Phys. Rev. B* **2010**, *82*, 104428.
(13) Patil, S.; Iyer, K. K.; Maiti, K.; Sampathkumaran, E. V. *Phys. Rev. B* **2008**, *77*, 094443.
(14) Bärnighausen, H.; Müller, U. Universität Karlsruhe and Universität-Gh Kassel, Germany, 1996.
(15) Bärnighausen, H. *Commun. Math. Chem.* **1980**, *9*, 139−175.
(16) Gordon, R. A.; Warren, C. J.; Alexander, M. G.; DiSalvo, F. J.; Pöttgen, R. *J. Alloys Compd.* **1997**, *248*, 24−32.
(17) Szlawska, M.; Kaczorowski, D. *Phys. Rev. B* **2011**, *84*, 094430.
(18) Chevalier, B.; Lejay, P.; Etourneau, J.; Hagenmuller, P. *Solid State Commun.* **1984**, *49*, 573.
(19) Kotsanidis, P. A.; Yakinthos, J. K.; Gamariseale, E. *J. Magn. Magn. Mater.* **1990**, *87*, 199−204.
(20) Majumdar, S.; Sampathkumaran, E. V.; Brando, M.; Hemberger, J.; Loidl, A. *J. Magn. Magn. Mater.* **2001**, *236*, 99−106.
(21) Sebastian, C. P.; Malliakas, C. D.; Chondroudi, M.; Schellenberg, I.; Rayaprol, S.; Hoffmann, R. D.; Pöttgen, R.; Kanatzidis, M. G. *Inorg. Chem.* **2010**, *49*, 9574−9580.
(22) Yubuta, K.; Yamamura, T.; Shiokawa, Y. *J. Phys. Condens. Matter* **2006**, *18*, 6109−6116.
(23) Takeda, N.; Ishikawa, M. *J. Phys. Soc. Jpn.* **1998**, *67*, 1062−1063.
(24) Szlawska, M.; Kaczorowski, D.; Reehuis, M. *Phys. Rev. B* **2010**, 81.
(25) Schroder, A.; Collins, M. F.; Stager, C. V.; Garrett, J. D.; Greedan, J. E.; Tun, Z. *J. Magn. Magn. Mater.* **1995**, *140*, 1407−1408.
(26) Li, D. X.; Shiokawa, Y.; Haga, Y.; Yamamoto, E.; Onuki, Y. *J. Phys. Soc. Jpn.* **2002**, *71*, 418−421.
(27) Li, D. X.; Donni, A.; Kimura, Y.; Shiokawa, Y.; Homma, Y.; Haga, Y.; Yamamoto, E.; Honma, T.; Onuki, Y. *J. Phys. Condens. Matter* **1999**, *11*, 8263−8274.
(28) Kaczorowski, D.; Noel, H. *J. Phys. Condens. Matter* **1993**, *5*, 9185−9195.
(29) Chevalier, B.; Pöttgen, R.; Darriet, B.; Gravereau, P.; Etourneau, J. *J. Alloys Compd.* **1996**, *233*, 150−160.
(30) Li, D. X.; Nimori, S.; Shiokawa, Y.; Haga, Y.; Yamamoto, E.; Onuki, Y. *Phys. Rev. B* **2003**, *68*, 012413.
(31) Li, D. X.; Nimori, S.; Shiokawa, Y.; Haga, Y.; Yamamoto, E.; Onuki, Y. *Phys. Rev. B* **2003**, *68*, 172405.
(32) Graw, G.; Bitterlich, H.; Loser, W.; Behr, G.; Fink, J.; Schultz, L. *J. Alloys Compd.* **2000**, *308*, 193−199.
(33) Kanatzidis, M. G.; Pöttgen, R.; Jeitschko, W. *Angew. Chem., Int. Ed.* **2005**, *44*, 6996−7023.
(34) Mazilu, I.; Frontzek, M.; Loser, W.; Behr, G.; Teresiak, A.; Schultz, L. *J. Cryst. Growth* **2005**, *275*, 103.
(35) Gladyshevskii, R. E.; Cenzual, K.; Parthe, E. *J. Alloys Compd.* **1992**, *189*, 221−228.
(36) Zhuravleva, M. A.; Kanatzidis, M. G. *J. Solid State Chem.* **2003**, *173*, 280−292.
(37) Zhuravleva, M. A.; Pcionek, R. J.; Wang, X. P.; Schultz, A. J.; Kanatzidis, M. G. *Inorg. Chem.* **2003**, *42*, 6412−6424.
(38) Zhuravleva, M. A.; Salvador, J.; Bilc, D.; Mahanti, S. D.; Ireland, J.; Kannewurf, C. R.; Kanatzidis, M. G. *Chem.—Eur. J.* **2004**, *10*, 3197−3208.
(39) Salvador, J. R.; Gour, J. R.; Bilc, D.; Mahanti, S. D.; Kanatzidis, M. G. *Inorg. Chem.* **2004**, *43*, 1403−1410.
(40) Salvador, J. R.; Malliakas, C. D.; Gour, J. R.; Kanatzidis, M. G. *Chem. Mater.* **2005**, *17*, 1636−1645.
(41) Wu, X. N.; Kanatzidis, M. G. *J. Solid State Chem.* **2005**, *178*, 3233.
(42) Chondroudi, M.; Balasubramanian, M.; Welp, U.; Kwok, W. K.; Kanatzidis, M. G. *Chem. Mater.* **2007**, *19*, 4769−4775.
(43) Sebastian, C. P.; Kanatzidis, M. G. *J. Solid State Chem.* **2010**, *187*, 2077.
(44) Sebastian, C. P.; Salvador, J.; Martin, J. B.; Kanatzidis, M. G. *Inorg. Chem.* **2010**, *49*, 10468−10474.

(45) Peter, S. C.; Chondroudi, M.; Malliakas, C. D.; Balasubramanian, M.; Kanatzidis, M. G. *J. Am. Chem. Soc.* **2011**, *133*, 13840−13843.
(46) Peter, S. C.; Rayaprol, S.; Francisco, M. C.; Kanatzidis, M. G. *Eur. J. Inorg. Chem.* **2011**, 3963−3968.
(47) Peter, S. C.; Malliakas, C. D.; Nakkotte, H.; Kothapilli, K.; Rayaprol, S.; Schultz, A. J.; Kanatzidis, M. G. *J. Solid State Chem.* **2012**, *187*, 200−207.
(48) Peter, S. C.; Kanatzidis, M. G. *Z. Anorg. Allg. Chem.* **2012**, *638*, 287−293.
(49) Chondroudi, M.; Peter, S. C.; Malliakas, C. D.; Balasubramanian, M.; Li, Q. A.; Kanatzidis, M. G. *Inorg. Chem.* **2011**, *50*, 1184−1193.
(50) Shigetoh, K.; Hirata, D.; Avila, M. A.; Takabatake, T. *J. Alloys Compd.* **2005**, *403*, 15−18.
(51) Gaudin, E.; Chevalier, B.; Heying, B.; Rodewald, U. C.; Pöttgen, R. *Chem. Mater.* **2005**, *17*, 2693−2700.
(52) Ivanshin, V. A.; Sukhanov, A. A.; Sokolov, D. A.; Aronson, M. C.; Jia, S.; Bud'ko, S. L.; Canfield, P. C. *J. Alloys Compd.* **2009**, *480*, 126−127.
(53) Kaczorowski, D.; Leithe-Jasper, A.; Rogl, P.; Flandorfer, H.; Cichorek, T.; Petri, R.; Andraka, B. *Phys. Rev. B* **1999**, *60*, 422−433.
(54) Murani, A. P. *NATO Sci. Ser. II Math.* **2003**, *110*, 297−305.
(55) Danzenbacher, S.; Kucherenko, Y.; Vyalikh, D. V.; Holder, M.; Laubschat, C.; Yaresko, A. N.; Krellner, C.; Hossain, Z.; Geibel, C.; Zhou, X. J.; Yang, W. L.; Mannella, N.; Hussain, Z.; Shen, Z. X.; Shi, M.; Patthey, L.; Molodtsov, S. L. *Phys. Rev. B* **2007**, *75*, 045109.
(56) Jeong, T.; Pickett, W. *J. Phys. Condens. Matter* **2006**, *18*, 6289−6297.
(57) Sheldrick, G. M. *Acta Crystallogr., Sect. A* **2008**, *64*, 112−122.
(58) *SHELXTL 5.10*; Bruker Analytical X-ray Systems, Inc.: Madison, WI, 1998.
(59) Gil, R. C.; Carrillo-Cabrera, W.; Schultheiss, M.; Peters, K.; von Schnering, H. G.; Grin, Y. *Z. Anorg. Allg. Chem.* **1999**, *625*, 285−293.
(60) Sheldrick, G. M. *SHELXTL, Structure Determination Program*, version 5; Siemens Analytical X-ray Instruments Inc.: Madison, WI, 1995.
(61) Zachwieja, U. *Z. Anorg. Allg. Chem.* **1996**, *622*, 1173−1176.
(62) Mullmann, R.; Mosel, B. D.; Eckert, H.; Pöttgen, R.; Kremer, R. K. *Hyperfine Interact.* **1997**, *108*, 389−400.
(63) Pöttgen, R. *J. Mater. Chem.* **1995**, *5*, 505−508.
(64) Pöttgen, R.; Borrmann, H.; Felser, C.; Jepsen, O.; Henn, R.; Kremer, R. K.; Simon, A. *J. Alloys Compd.* **1996**, *235*, 170−175.
(65) Pöttgen, R.; Borrmann, H.; Kremer, R. K. *J. Magn. Magn. Mater.* **1996**, *152*, 196−200.
(66) Rossi, D.; Marazza, R.; Ferro, R. *J. Alloys Compd.* **1992**, *187*, 267−270.
(67) Schnelle, W.; Pöttgen, R.; Kremer, R. K.; Gmelin, E.; Jepsen, O. *J. Phys. Condens. Matter* **1997**, *9*, 1435−1450.
(68) Merlo, F.; Pani, M.; Canepa, F.; Fornasini, M. L. *J. Alloys Compd.* **1998**, *264*, 82−88.
(69) Donohue, J. *The Structures of the Elements*; Wiley: New York, 1974.
(70) Buzaneva, E.; Scharff, P. *Frontiers of Multifunctional Nanosystems*; Kluwer Academic Publishers: Dordrecht Netherlands, 2002; p 293.
(71) Kambe, S.; Suderow, H.; Fukuhara, T.; Flouquet, J.; Takimoto, T. *J. Low Temp. Phys.* **1999**, *117*, 101−112.
(72) Coleman, P. *Introduction to Many Body Physics*; Rutgers University Press: New Jersey, 2004.
(73) Li, S. Y.; Taillefer, L.; Hawthorn, D. G.; Tanatar, M. A.; Paglione, J.; Sutherland, M.; Hill, R. W.; Wang, C. H.; Chen, X. H. *Phys. Rev. Lett.* **2004**, *93*, 056401.
(74) Varma, C. M. *Rev. Mod. Phys.* **1976**, *48*, 219.
(75) Sereni, J. G.; Caroca-Canales, N.; Kumar, M.; Oeschler, N.; Berisso, M. G.; Geibel, C. *J. Phys. Conf. Ser.* **2010**, *200*, 012181.
(76) Rebelsky, L.; Reilly, K.; Horn, S.; Borges, H.; Thompson, J. D.; Willis, J. O.; Aikin, R.; Caspari, R.; Bredl, C. D. *J. Appl. Phys.* **1988**, *63*, 3405−3407.
(77) Gopal, E. S. R. *Specific heat at low temperatures*; Plenum: New York, 1966.
(78) Goltsev, A. V.; Golubkov, A. V.; Smirnov, I. A.; Misiorek, H.; Sulkovski, C. *Phys. Solid State* **2006**, *48*, 622−624.
(79) Tsujii, N.; Kontani, H.; Yoshimura, K. *Phys. Rev. Lett.* **2005**, *94*, 057201−057204.
(80) Tsujii, N.; Kontani, H.; Yoshimura, K. *J. Phys. Soc. Jpn.* **2007**, *76*, 174−177.